Colloids and Surfaces A: Physicochem. Eng. Aspects 371 (2010) 104–112

Contents lists available at ScienceDirect

Colloids and Surfaces A: Physicochemical and Engineering Aspects

journal homepage: www.elsevier.com/locate/colsurfa

Nanosized magnetofluorescent Fe_3O_4–curcumin conjugate for multimodal monitoring and drug targeting

Lam Dai Tran[a,*,1], Nhung My T. Hoang[b,1], Trang Thu Mai[a], Hoang Vinh Tran[c], Ngoan Thi Nguyen[d], Thanh Dang Tran[a], Manh Hung Do[a], Qui Thi Nguyen[b], Dien Gia Pham[d], Thu Phuong Ha[a], Hong Van Le[a], Phuc Xuan Nguyen[a,*,1]

[a] Institute of Materials Science, Vietnam Academy of Science and Technology, 18 Hoang Quoc Viet, Hanoi, Viet Nam
[b] Faculty of Biology, Hanoi University of Science, Vietnam National University, 334 Nguyen Trai, Hanoi, Viet Nam
[c] Faculty of Chemical Technology, Hanoi University of Technology, 1 Dai Co Viet, Hanoi, Viet Nam
[d] Institute of Chemistry, Vietnam Academy of Science and Technology, 18 Hoang Quoc Viet, Hanoi, Viet Nam

ARTICLE INFO

Article history:
Received 4 June 2010
Received in revised form 18 August 2010
Accepted 9 September 2010
Available online 17 September 2010

The authors dedicate this publication to Prof. Acad. Nguyen Van Hieu, father of Vietnam Nanotechnology, in celebration of his 72nd birthday.

Keywords:
Magnetofluorescent Fe_3O_4
Curcumin (Cur)
Macrophages
Chitosan (CS)
Oleic acid (OL)
Laser scanning confocal microscope (LSCM)
Physical properties measurement systems (PPMS)

ABSTRACT

Magnetic drug targeting, the targeting of a drug conjugated with a magnetic material under the action of external magnetic field constitutes an important drug delivery system. This paper describes the strategy to design a multifunctional, nanosized magnetofluorescent water-dispersible Fe_3O_4–curcumin conjugate and its multiple ability to label, target and treat the tumor cells. The conjugate possesses magnetic nano Fe_3O_4 core, chitosan (CS) or oleic acid (OL) as outer shell and entrapped curcumin (Cur), serving dual function of naturally autofluorescent dye as well as anti-tumor model drug, delivered to the cells with the help of macrophage (Cur possesses anti-oxidant, anti-inflammatory and anti-tumor ability). Fe_3O_4–Cur conjugate exhibited a high loading cellular uptake which was clearly visualized dually by Fluorescence Microscope, Laser scanning confocal microscope (LSCM) as well as magnetization measurement (Physical properties measurement systems, PPMS). Preliminary magnetic resonance imaging (MRI) study also showed a clear contrast enhancement by using Fe_3O_4–Cur conjugate.

1. Introduction

Magnetic nanoparticles (MNPs) with an appropriate surface modification have been widely used for numerous biomedical applications [1–15]. In nanomedicine, MNPs can be used either in diagnostic (magnetic resonance imaging contrast agents and magnetic enhanced enzyme-linked immunoassay) and in therapeutic (drug delivery and hyperthermia) applications, for which it is required that the MNPs have high magnetization value, small size, and special surface coating by a non-toxic, biocompatible layer.

Surface coatings provide a steric barrier to prevent nanoparticle agglomeration and avoid opsonization (the uptake by the reticuloendothelial system (RES), thus shortens circulation time in the blood and MNP's ability to target the drug to specific sites and reduce side effects). In addition, these coatings provide a means to tailor the surface properties of MNPs such as surface charge and chemical functionality. Some critical aspects with regard to polymeric coatings that may affect the performance of an MNP system include the nature of the chemical structure of the polymer (e.g. hydrophilicity/hydrophobicity, biodegradation), its molecular weight and conformation, the manner in which the polymer is anchored or attached (e.g. electrostatic, covalent bonding) and the degree of particle surface coverage. A variety of natural polymers/surfactants have been evaluated for this purpose. The most widely utilized and successful coatings, in terms of *in vivo* applications, are dextran, PEG, chitosan (CS) and oleic acid (OL) [16–19].

Monocytes and macrophages are phagocytes, acting in both non-specific defense (innate immunity) as well as to help initiate specific defense mechanisms (adaptive immunity) of vertebrate animals. Their role is to phagocytise (engulf and then digest) cel-

* Corresponding authors. Tel.: +84 4 37564129; fax: +84 438360705.
E-mail addresses: lamtd@ims.vast.ac.vn (L.D. Tran), phucnx@ims.vast.ac.vn (P.X. Nguyen).
[1] These authors equally contributed to this paper.

0927-7757/$ – see front matter © 2010 Elsevier B.V. All rights reserved.
doi:10.1016/j.colsurfa.2010.09.011

lular debris and pathogens either as stationary or as mobile cells, and to stimulate lymphocytes and other immune cells to respond to the pathogen [20]. Hence, they can be used as potential vehicles for transport of MNPs into the core of tumor cells.

In this study, we do not take upon ourselves to introduce novel coating materials but emphasize our efforts on designing stable conjugates for their application *in vivo*, namely for imaging and drug targeting. Because MNPs that have a highly hydrophilic surface resist well to opsonizations and therefore are cleared slowly, our choice was based on well known hydrophilic chitosan (CS) and oleic acid (OL), rationalizing on the fact that CS is an excellent biocompatible biodegradable polymer with a high content of amino groups ($-NH_2$) that makes possible complexation reaction with metal ions in solution and other chemical reactions with the purpose of improving polymeric surface modification and drug delivery. As for OL, a wide spread substance in nature, it is intensively investigated in different aspects of its biological actions owing to the absence of its chronic adverse health effects and toxicity.

The aim of this work is first to fabricate Fe_3O_4–Cur conjugates with diameter < 500 nm, coated by CS or OL, and then to use macrophage as a vehicle to carry these conjugates into tumor. Being non-toxic, autofluorescent and anti-cancerous, Cur would play a role of multifunctional probe in Fe_3O_4–Cur uptake visualization/monitoring by two complementary methods of fluorescent and magnetic imaging. To our best knowledge, it may be the first study reported about the original characteristics and application of Cur in cellular imaging and drug targeting.

2. Experimental

2.1. Chemical and biochemical materials

All the chemicals were of reagent grade used without further purification. Ferric chloride hexa-hydrate ($FeCl_3{\cdot}6H_2O$), ferrous chloride tetra-hydrate ($FeCl_2{\cdot}4H_2O$), NaOH, NH_4OH (26% of ammonia), oleic acid ($C_{17}H_{33}COOH$) were purchased from Aldrich. Chitosan (MW = 400.000, DA = 70%) was purchased from Nha Trang Aquatic Institute (Vietnam) and re-characterized by viscometry and IR measurements at our laboratory. Curcumin (1,7-bis(4-hydroxy-3-methoxyphenyl)-1,6- heptadiene-3,5-dione) was from Institute of Chemistry (Vietnam).

Cells were cultured in RPMI 1640 (Roswell Park Memorial Institute) (Gibco) medium. This medium was supplemented with 10% fetal bovine serum (Invitrogen), 100 IU/ml penicillin–streptomycine (Invitrogen), 2 mM–glutamine (Invitrogen). Cells were grown in a humidified chamber in the presence of 5% CO_2, at 37 °C.

Human Buffy coat was obtained from National Institute of Hematology and Transfusion (Vietnam). Mononuclear cells were isolated by density gradient centrifugation using 1.077 g/ml Ficoll. Cells were cultured in RPMI 1640 medium with 1 μg/ml HGM-CSF (human granulocyte macrophage-colony stimulating factor) (MP Biomedicals). 7–12-week-old Swiss mice were obtained from National Institute of Hygiene and Epidemiology (Vietnam). Primary peritoneal macrophages isolation was described in details elsewhere [21]. Human monocytes or mouse primary peritoneal macrophages were grown for 24 h on glass coverslips. 10^6 cells were incubated with 0.05 mg MNPs for 2–15 h, then treated with either anti-human CD14 antibody (Bio Legend) or actins antibody (Invitrogen) for taking LSCM images.

2.2. Fe_3O_4–Cur conjugate preparation

CS-coated Fe_3O_4 fluid (CSF) was prepared by chemical co-precipitation of Fe^{2+} and Fe^{3+} ions by NaOH in the presence of CS according to the detailed procedure, described in [22]. OL coated Fe_3O_4 fluid (OLF) was prepared with multistep synthesis [23]. Briefly, OLF and CSF were synthesized by the co-precipitation from iron chloride solution (with Fe^{3+}/Fe^{2+} ratio of 2:1. Then, Cur (preliminarily solubilized in ethanol) was attached by adsorption on the Fe_3O_4 surface of OLF/CSF. Thus, several types of ferrofluid without/with Curcumin (Cur) have been prepared for further fluorescent and magnetic imaging: (i) OLF; (ii) CSF; (iii) OLF–Cur; (iv) CSF–Cur.

2.3. Characterization methods

Infra red (IR) spectra were recorded with Nicolet 6700 FT-IR Spectrometer, using KBr pellets, in the region of 400–4000 cm^{-1}, with resolution of 4 cm^{-1}. Field emission scanning electron microscope (FE-SEM) and Transmission electron microscope (TEM) images were analyzed by Hitachi S-4800 and JEM-1200EX (Voltage:100 kV, magnification X200,000), respectively. Dynamic light scattering (DLS) was analyzed with Zetasizer 2000 instrument (Malvern, UK).

Ultraviolet–visible (UV–vis) spectra were recorded by UV–vis Agilent 8453 spectrophotometer in the range of 250–800 nm; fluoresence spectra were recorded by using Jobin-Yvon FL3-22.

Laser scanning confocal microscope (LSCM) images with excitation light of 488 nm were collected with use of a ZEISS 510 LSCM with a 20× or 40× or 63× oil immersion objectives.

The magnetic properties were measured using Physical properties measurement system (PPMS) from Quantum Design at fields ranging from −20 to 20 kOe at 25 °C, with accuracy of 10^{-5} emu.

The images of mice tumor were carried out by Philips Intera 1.5 T MR scanner (Netherlands) with the slice thickness of 3 mm on transversal and coronal planes, and using two sequences – T2-weighted and T1-weighted.

3. Results and discussion

3.1. Size and structural characterizations of conjugates

DLS and TEM/FE-SEM data indicated that hydrodynamic diameters of OLF; CSF; OLF–Cur and CSF–Cur are ca. 10 nm, 30 nm, 300 nm and 500 nm, respectively (Fig. 1). First, the significant increase in size of OLF–Cur and CSF–Cur, compared to those of OLF and CSF respectively can be associated with the core- shell expansion after Cur loading. Second, although being in satisfactory agreement, slight discrepancy of TEM/FE-SEM data compared to DLS result can be understood if taking into account the fact that TEM/FE-SEM images are taken in a dried state and outer coatings could result in differences in measured particle diameters. Third, FE-SEM micrographs also confirmed the different morphologies between OLF–Cur (Fig. 1c) and CSF–Cur (Fig. 1d): OLF–Cur conjugates showed a quite strong tendency to form big aggregates whose sizes (300 nm) are much greater than those of isolated (primary) particles (ca.50 nm) or their cluster; as for CSF–Cur, the degree of agglomeration is much less important; however, the conjugates with bigger size (350–450 nm) were formed. FE-SEM pattern is well consistent with what is monitored in DLS measurement. In DLS graph of OLF–Cur: two distinct peaks, corresponding to the difference in size of aggregated (bigger) and isolated (smaller) clusters, respectively were clearly observed (Fig. 1c, left image), while only one peak was observed in case of CSF–Cur (Fig. 1d, left image). A crucial difference between structural nature of OL and CS may explain why OLF–Cur and CSF–Cur had that different degree of agglomeration.

Next, IR spectra were recorded to elucidate the interaction mechanism between Fe_3O_4 core and protective shell of OL and CS. As for OL, it was observed that the vibration at 1730 cm^{-1} on spectrum of the pure OL disappeared, while a new peak at 1644 cm^{-1}

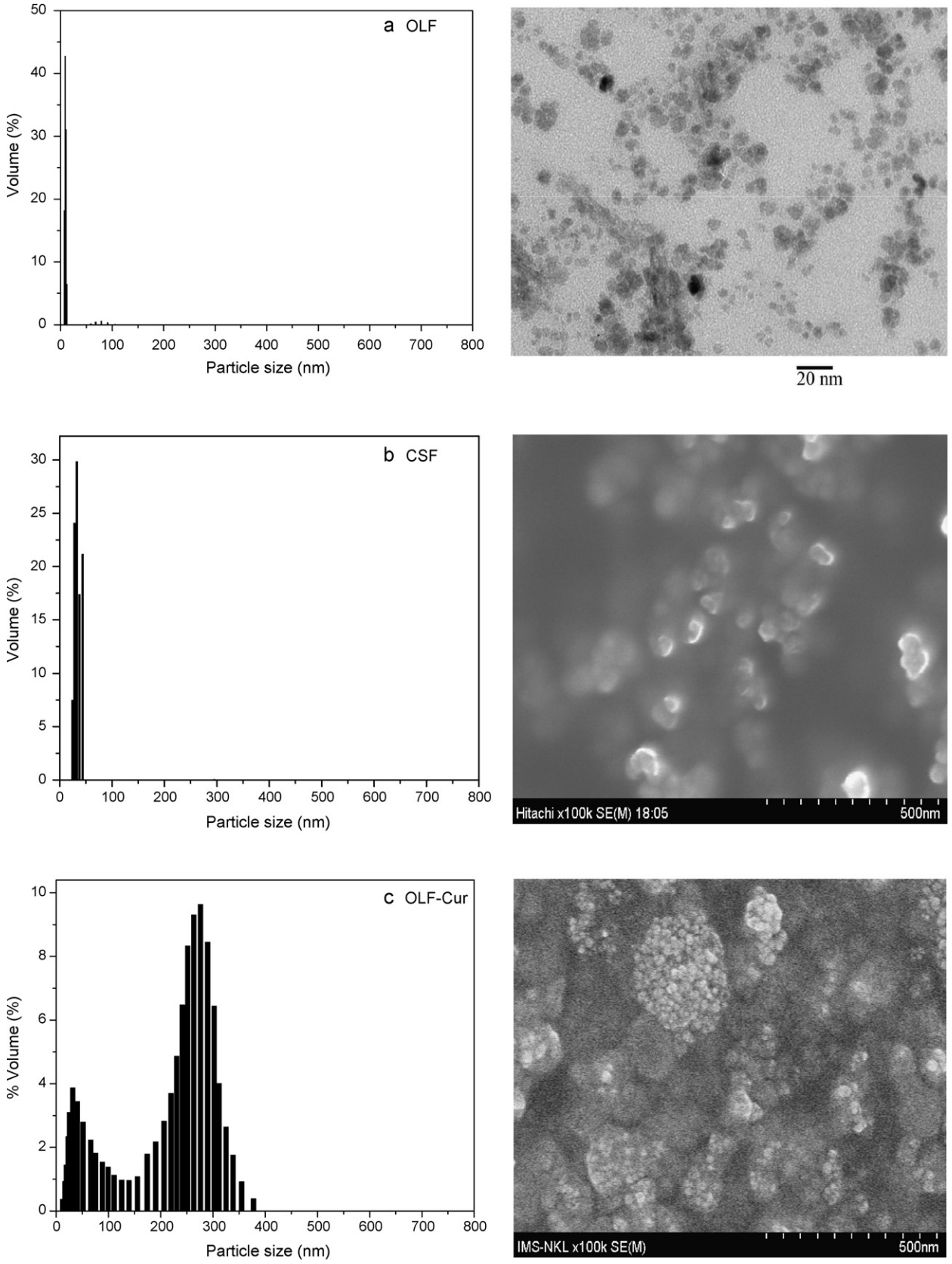

Fig. 1. Dynamic light scattering (DLS) spectra and corresponding TEM or FE-SEM images of 4 Fe_3O_4 fluids: OLF (a); CSF (b); OLF–Cur (c); and CSF–Cur (d).

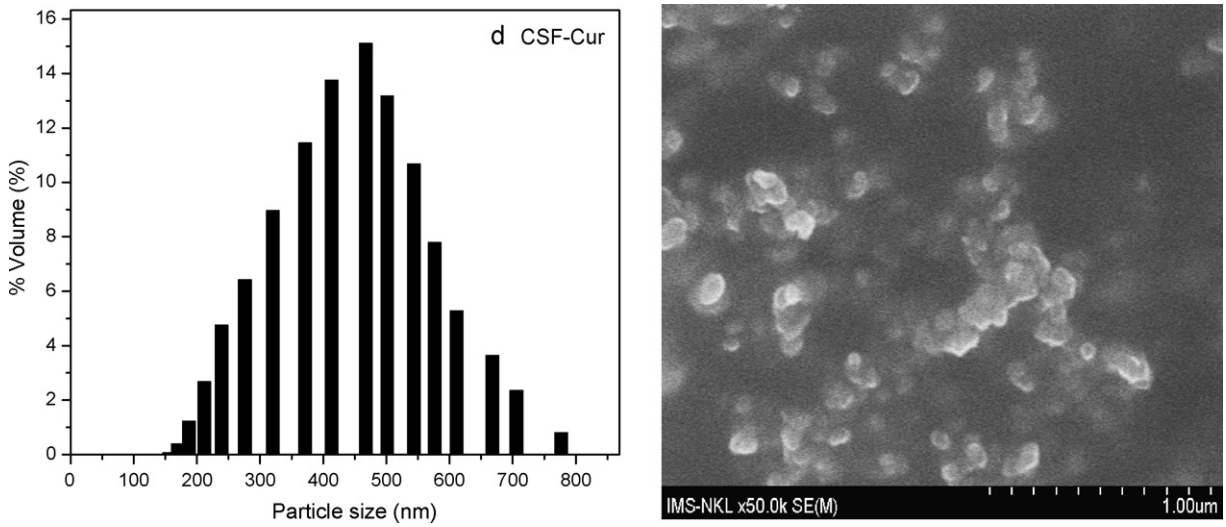

Fig. 1. (*Continued*).

assigned for symmetric (COO^-) stretches was pronounced. This shift can be explained as COO^- of OL chemisorbed onto Fe atoms on the surface of Fe_3O_4 nanoparticles and rendered a partial single bond character of the C=O bond to weaken it, and thus shift the stretching frequency to a lower value (Fig. 2). In the case of CSF–Cur, IR spectra demonstrated the fingerprint band shift of bending vibration of δ(N–H) from 1638 to 1681 cm^{-1}, indicating binding of iron ions to NH_2 group of CS (Fig. 3).

Further, compared with IR spectrum of pure Cur, IR spectra of OLF–Cur and CSF–Cur showed a significant change (peak form and position) in the range of 3600–3500 cm^{-1}, which was assigned to the vibration of –OH group of Cur and adsorbed water (aqueous medium). While free Cur showed a strong sharp O–H stretch at 3512 cm^{-1}, broad O–H stretch of OLF–Cur and CSF–Cur probably indicated about strong hydrogen bonding due to the formation of intermolecular bonding between OL or CS and Cur. Additionally, the characteristic peaks of Cur at 1525, 1280, 960 cm^{-1} (with insignificant peak shifts) [24,25], observed on the spectra of OLF–Cur and CSF–Cur, strongly confirmed the presence of Cur in OLF–Cur and CSF–Cur.

Next, UV–vis spectrum of OLF–Cur conjugate showed absorption maximum at 429 nm assigned to the band $\pi \rightarrow \pi^*$ of Cur (Fig. 4). Compared with pure Cur (maximum absorption located at 424 nm), the conjugate showed a maximum absorption shift of 4–5 nm. No other peaks or shoulders could be detected, potentially meaning that no Cur → (Fe^{2+}) charge transfer was formed. This UV absorption effect is consistent with green fluorescence image, as demonstrated in Fig. 5 for the OLF-Cur sample measured by fluorescence microscope. As shown in Fig. 6, the fluorescence emission peak of OLF–Cur was shifted compared to that of free Cur ($\Delta\lambda$ = 8 nm). Considering the fact that the fluorescence spectrum of a compound is usually affected by its microenvironment, this result further confirmed that the microenvironment of OLF–Cur was changed after conjugation of OLF with Cur [26] and OLF–Cur conjugate remains a strong fluorescence intensity that is very important for its application as fluorescence probe for drug targeting visualization (see Section 3.3).

3.2. Magnetic properties

Fig. 7 presents the $M(H)$ curves taken for CSF and CSF–Cur. On the basis of saturation magnetization values of non coated Fe_3O_4 NPs (70 emu/g) [23], CSF (1.225 emu/g) and CSF–Cur (1.209 emu/g),

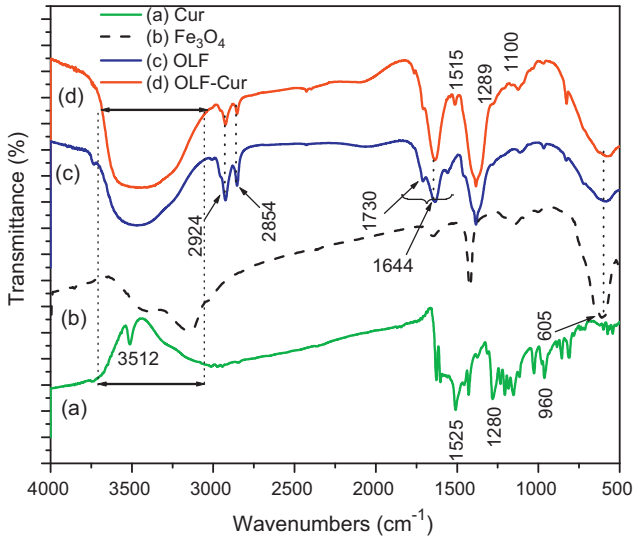

Fig. 2. IR spectra of free Cur (a); Fe_3O_4 (b); OLF (c); and Cur-containing OLF–Cur (d) fluids.

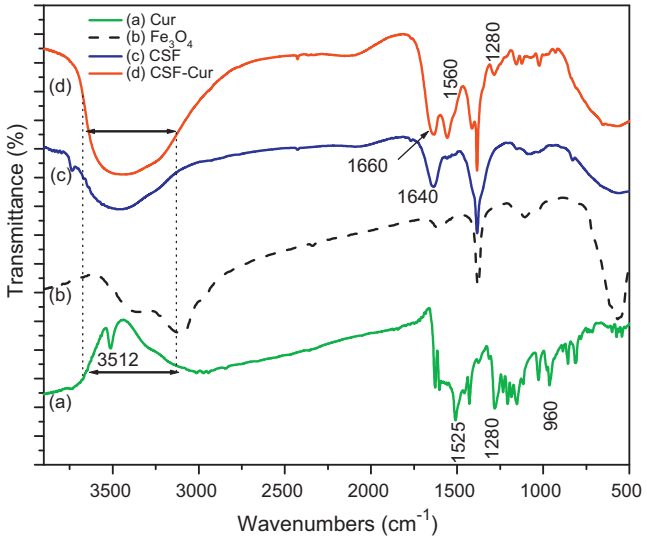

Fig. 3. IR spectra of free Cur (a); Fe_3O_4 (b); CSF (c); and Cur-containing CSF–Cur (d) fluids.

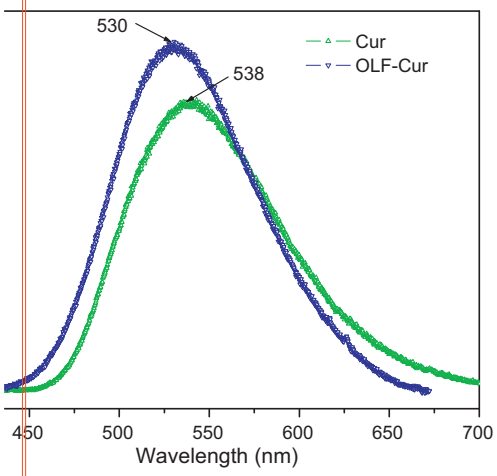

ence spectra of free Cur and Cur-containing OLF–Cur fluid.

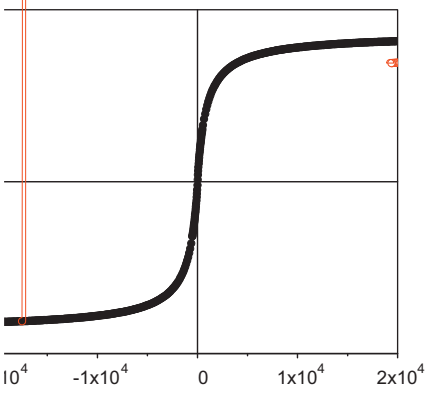

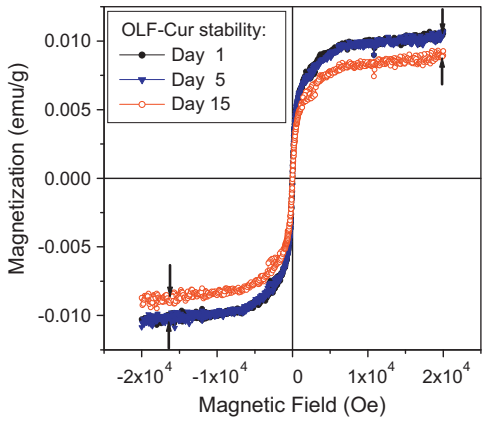

Fig. 8. Magnetic stability of the diluted OLF–Cur fluids in PBS (pH 7.4).

drug and the drug uptake can be observed *in situ* either by fluorescence or by magnetic measurements without the use of external fluorescent label such as toxic CdS type quantum dots.

First, as may be seen from Fig. 9, a strong accumulation of green spots of Cur in the cytoplasm was observed and that phenomenon could be explained by the fact that OLF–Cur and CSF–Cur conjugates were considered by macrophages as a pathogen agent (on the fluorescence images the conjugate localization was visualized by green fluorescence of Cur, actin proteins and nucleus were colored by Red Texas and blue respectively). Next, the uptake of the conjugate by human monocytes-derived macrophages (Fig. 9b) is less than that induced by mouse primary peritoneal ones (Fig. 9c), probably due to the higher activity of peritoneal macrophages compared to those differentiated from peripheral blood monocytes in vitro. Further, it is very important to note that fluorescent signals of OLF–Cur (Fig. 9d) were much stronger than those of CSF–Cur (Fig. 9c) and they were not randomly nor equally distributed in cells as would be in the case of non-specific adsorption of Cur-containing conjugates on the cell surface but predominantly enriched in the cell cytoplasm.

Uptake of OLF–Cur by macrophage was also seen by TEM. TEM images of control (Fig. 10a) and treated cells with OLF (Fig. 10b) also showed a pronounced accumulation of conjugates in the cells. Effectively, as for OLF–Cur loaded macrophages, as a result of cell activation, the cells had more irregular nuclear shape, more voluminous cytoplasm with numerous vacuoles and bigger size, compared to the normal, untreated cells.

Further, to get closer insights into the kinetics, Fe_3O_4–Cur uptake was visualized by LCSM *in situ* images, taken at 1, 2, 4, 6 h of OLF–Cur incubation. As expected, the number of Fe_3O_4–Cur

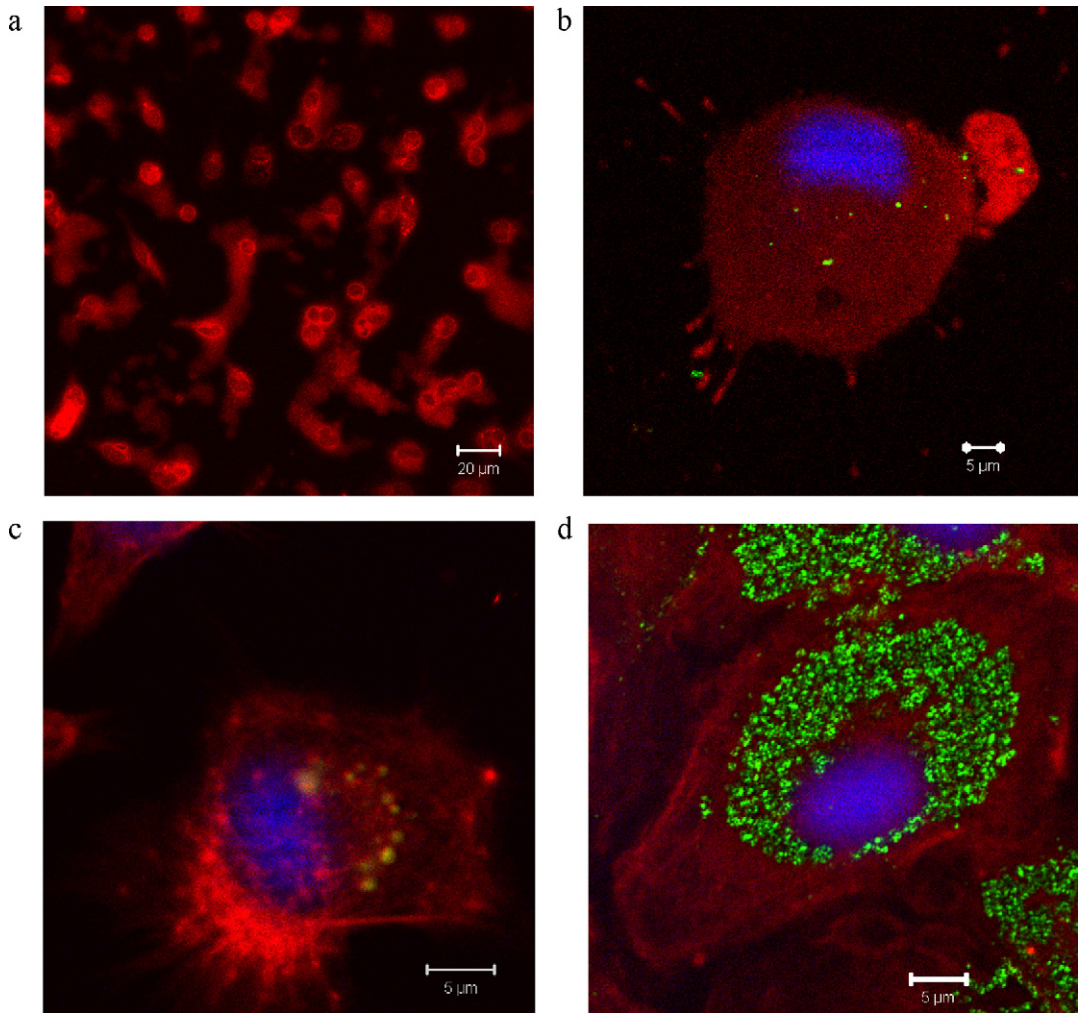

Fig. 9. Cellular uptake of CSF–Cur and OLF–Cur conjugates by macrophages. (a) Primary cultures of monocytes-derived macrophages stained for CD14 antigen (red). (b) Phagocytosis of CSF–Cur by human monocytes-derived macrophages. (c) Phagocytosis of CSF–Cur by mouse macrophages. (d) Phagocytosis of OLF–Cur by mouse macrophages. (Nanoparticles localization is visualized by autofluorescence of Cur. Actin is colored by Red Texas and nucleus is in blue (b, c, d)). (For interpretation of the references to color in this figure legend, the reader is referred to the web version of the article.)

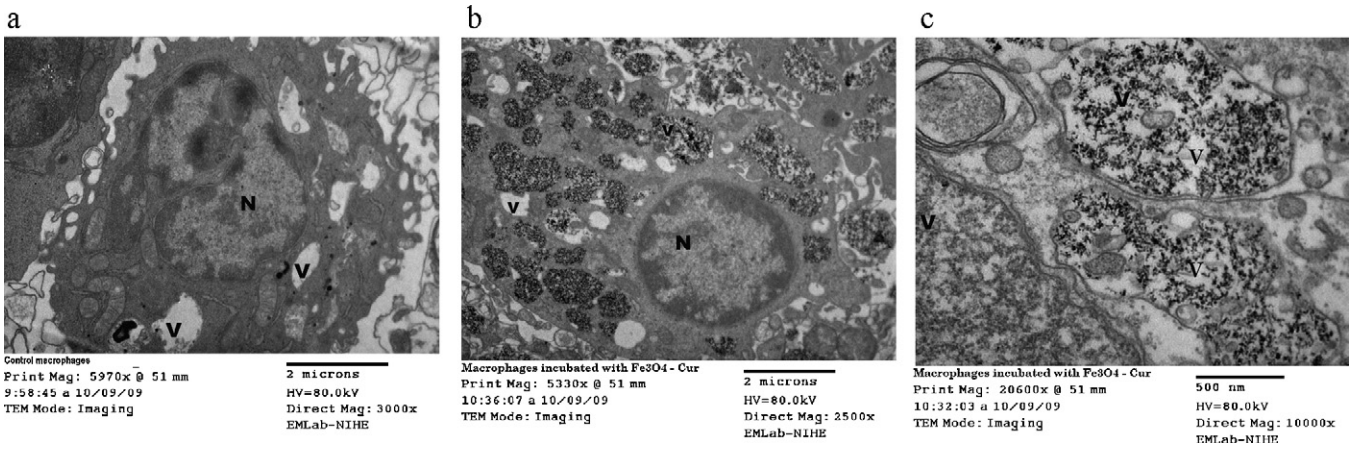

Fig. 10. TEM images of the control (without incubation with OLF–Cur) mouse macrophage (a) and OLF–Cur loaded mouse macrophages (b, c). N and V stand for nucleus and vacuole respectively.

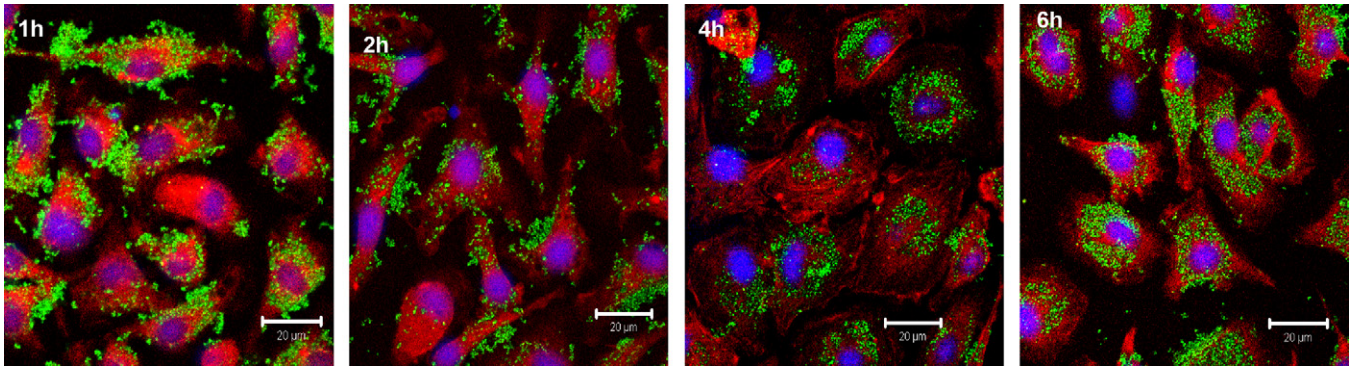

Fig. 11. Cellular uptake kinetic monitoring of OLF–Cur observed by *in situ* LSCM (taken at 1, 2, 4 and 6 h).

uptaken into macrophage cytoplasm increases clearly with increasing incubation time. The green fluorescent color is noticeably seen surrounding the nucleus surface at 0.5–1 h, then appears increasingly inside the nucleus at 2–4 h and finally reaches its maximal intensity there at 6 h. Since fluorescencent intensity of Cur directly correlates to the internalization ability of Fe_3O_4–Cur into cells, it can be concluded that the Fe_3O_4–Cur particles are efficiently internalized (Fig. 11).

In addition to *in situ* LSCM measurement, PPMS magnetization experiments (pseudo *in situ* measurements) were carried out by "interrupted sampling and measuring" at different times. It is observed that for both OLF–Cur and CSF–Cur, the magnetization of macrophage increases with increasing time of incubation (accordingly, the magnetization of the remaining supernatant decreases with the time). Fig. 12 presents magnetization curves of macrophage samples at four different t (t = 1 h, 2 h, 4 h and 6 h) of OLF–Cur conjugate incubation. This magnetization result is, therefore, in good accordance with that done by the above demonstrated *in situ* observation by LSCM fluorescence.

3.4. Preparation of tumor-bearing mice and MR images

Mouse Sarcoma −180 cells were suspended at 5×10^6 cells in 1 ml of PBS, pH 7.2. To prepare tumor-bearing mice, the suspension of 0.2 ml was transplanted subcutaneously into the right femoral region of each Swiss mouse under short-term anesthesia by intra-peritoneal injection of thiopental. On the 9–11 days after transplantation, when tumors have the size of about 8 mm × 11 mm the nanoparticles (OLF–Cur) were introduced to tumors by intra-tumor injection directly. A healthy mouse and a tumor-bearing mouse injected with the equivalent volume of PBS were used as control. The mice were, then, imaged by the Philips Intera 1.5 Tesla MR scanner with the slice thickness of 3 mm on transversal using T2-weighted sequences. Each scanning took about 5–7 min. Fig. 13 presents 3 images of a mouse bearing a Sarcoma tumor at its right femora. While there was almost no significant difference in tumor signal intensity as com-

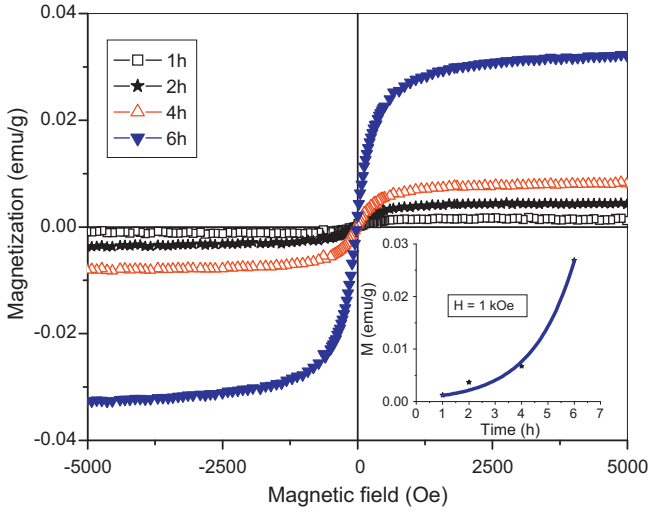

Fig. 12. Cellular uptake kinetic monitoring of OLF–Cur observed by pseudo *in situ* PPMS measurement (measured at 1,2, 4 and 6 h). Inset: Magnetization value vs. time at 1 kOe.

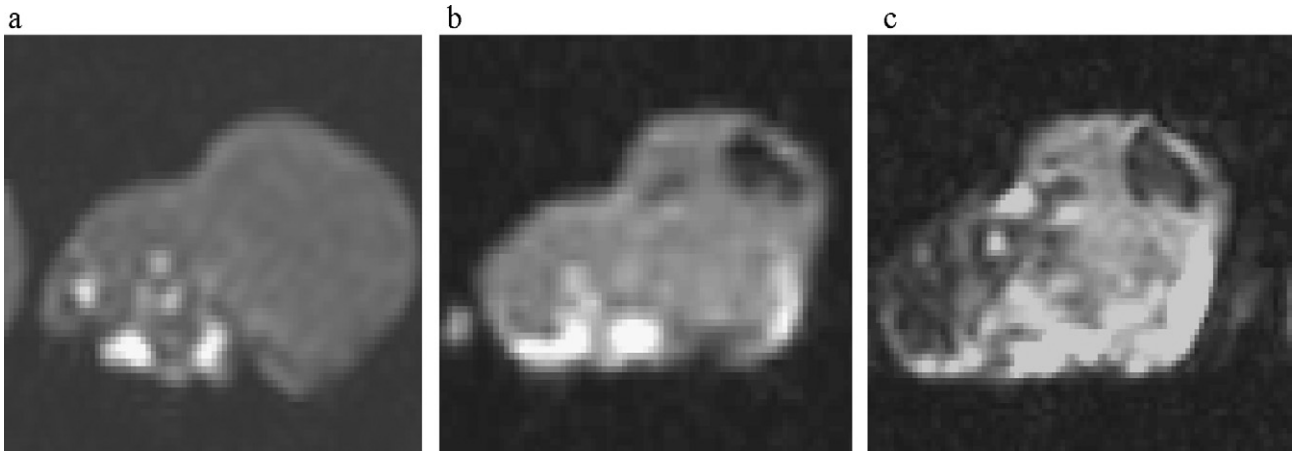

Fig. 13. MR images of a tumor region measured: before direct OLF–Cur injection (a); 1 min after OLF–Cur injection (b); and 5 min after OLF–Cur injection (c).

pared with control (image *a*), the intra-tumor injection of OLF–Cur resulted in reducing the MR signal intensity, which in turn made the invaded region black (images *b* and *c*). Owing to this contrast change the tumor can be easily differentiated from the surrounding tissues.

4. Conclusion

This paper presents a simple chemical conjugation route to functionalize Fe_3O_4 surface and incorporate Cur, a natural fluorescent dye and anti-cancer drug onto these magnetic nanoparticles, and its demonstration as a potentially multimodal probe for fluorescence as well as magnetic (PPMS, MR) observation. Ability of phagocytosis of the OLF–Cur and CSF–Cur by either human monocytes-derived or mouse primary peritoneal macrophages was clearly observed by magnetic and fluorescent methods. The conjugates also showed to be a good candidate for a dual (optical and magnetic) imaging probe. Although not fully interpreted, the results are promising. Further developments in particle synthesis for more efficient capture and targeting and novel improved strategies for localizing cancerous tumors will be reported in the next study.

Acknowledgments

The authors are grateful for the financial support for this work by application oriented basic research project (2009–2012, code 01/09/HD-DTDL), Korean–Vietnamese joint research project (2010–2011, code 59/2615/2010/HD-NDT). The authors would like to acknowledge their indebtedness to Prof. Nguyen Quang Liem and all members of IMS-VAST key laboratory for providing lab's facilities; Dr. N.T.K.Thanh (Davy-Faraday Research Laboratory, U.K) for her reading to early version of this manuscript.

References

[1] A. Kumar, P.K. Jena, S. Behera, R.F. Lockey, S. Mohapatra, S. Mohapatra, Multifunctional magnetic nanoparticles for targeted delivery, nanomedicine, nanotechnology, Biology and Medicine 6 (2010) 64–69.
[2] A.H. Lu, E.L. Salabas, F. Schuth, Magnetic nanoparticles: synthesis, protection, functionalization, and application, Angewandte Chemie International Edition 46 (2007) p.1222–1244.
[3] Q.A Pankhurst, N.K.T. Thanh, S.K. Jones, J. Dobson, Progress in applications of magnetic nanoparticles in biomedicine, Journal of Physics D: Applied Physics 42 (2009) 224001–224014.
[4] P. Moroz, S.K. Jones, B.N. Gray, Magnetically mediated hyperthermia: current status and future direction, International Journal of Hyperthermia 18 (2002) 267–284.
[5] U. Gneveckow, A. Jordan, R. Scholz, V. Bruss, N. Waldofner, Description and characterization of the novel hyperthermia- and thermoablation-system MFH® 300F for clinical magnetic fluid hyperthermia, Medical Physics 31 (2004) p.1444–1451.
[6] B. Koppolu, M. Rahimi, S. Nattama, A. Wadajkar, K.T. Nguyen, Development of multi-layer polymeric particles for targeted and controlled drug delivery, nanomedicine, nanotechnology, Biology and Medicine 6 (2010) 355–361.
[7] T.R. Sathe, A. Agrewal, S. Nie, Mesoporous silica beads embedded with semiconductor quantum dots and ion oxide nanocrystals: dual-function microcarriers for optical encoding and magnetic separation, Analytical Chemistry 78 (2006) 5627–5632.
[8] M. Yanase, M. Shinkai, H. Honda, T. Wakabayashi, J. Yoshida, T. Kobayashi, Intracellular hyperthermia for cancer using magnetite cationic liposemes: an in vivo study, Japanese Journal of Cancer Research 89 (1998) 463–470.
[9] C.C. Berry, A.S.G. Curtis, Functionalization of magnetic nanoparticles for applications in biomedicine, Journal of Physics D: Applied Physics 36 (2002) R167–R181.
[10] T.K. Jain, S.P. Foy, B. Erokwu, S. Dimitrijevic, C.A. Flask, V. Labhasetwar, Magnetic resonance imaging of multifunctional pluronic stabilized iron-oxide nanoparticles in tumor-bearing mice, Biomaterials 30 (2009) p.6748–6756.
[11] A. Zhu, L. Yuan, W. Jin, S. Dai, Q. Wang, Z. Xue, A. Qin, Polysacharide surface modified Fe_3O_4 nanoparticles for canaptothecin loading and delivery, Acta Biomaterialia 5 (2009) 1489–1498.
[12] K.J. Widder, A.E. Senyel, G.D. Scarpelli, Magnetic microspheres: a model system of site specific drug delivery in vivo, in: Proceedings of the Society for Experimental Biology and Medicine, 1978, pp. 141–146, 158.
[13] D. Kropke, R.A. Wassel, F. Mondalek, B. Grady, K. Chen, J.Z. Liu, D. Gibson, K.J. Dormer, Magnetic nanoparticles: inner ear targeted molecule delivery and middle ear implant, Audiology and Neurotology 11 (2006) 123–133.
[14] S. Bisht, G. Feldmann, S. Sony, R. Ravi, C. Karikar, A. Maitra, A. Maitra, Polymeric nanoparticle-encapsulated curcumin ("nanocurcumin"): a novel strategy for human cancer therapy, Journal of Nanobiotechnology 5 (2007), doi:10.1186/1477-3155-5-3.
[15] K. Sou, S. Inenaga, S. Takeoka, E. Tsuchida, Loading of curcumin into macrophages using lipid-based nanoparticles, International Journal of Pharmaceutics 352 (2008) 287–293.
[16] G.Y. Li, Y.R. Jiang, K.L. Huang, P. Ding, J. Chen, Preparation and properties of magnetic Fe_3O_4–chitosan nanoparticles, Journal of Alloys and Compounds 466 (2008) 451–456.
[17] P.R. Gil, D. Hühn, L.L. del Mercato, D. Sasse, W.J. Parak, Nanopharmacy: Inorganic nanoscale devices as vectors and active compounds, Pharmacological Research, in press, doi:10.1016/j.phrs.2010.01.009.
[18] M. Rutnakkornpituk, S. Meerod, B. Boontha, U. Wichai, Magnetic core–bilayer shell nanoparticle: a novel vehicle for entrapment of poorly water-soluble drugs, Polymer 50 (2009) 3508–3515.
[19] T. Rheinlander, R. Kotitz, W. Weitschies, W. Semmler, Different methods for the fractionation of magnetic fluids, Colloid & Polymer Science 278 (2000) 259–263.
[20] M. Muthana, S.D. Scott, N. Farrow, F. Morrow, C. Murdoch, S. Grubb, N. Brown, J. Dobson, A nove magnetic approach to enhance the efficacy of cell based gene therapies, Gene Therapy 15 (2008) 902–910.
[21] J.G. Kim, C. Keshava, A.A. Murphy, R.E. Pitas, S. Parthasarathy, Fresh mouse peritoneal macrophages have low scavenger receptor activity, Journal of Lipid Research 38 (1997) 2207–2215.
[22] H.V. Tran, L.D. Tran, T.N. Nguyen, Preparation of chitosan/magnetite composite beads and their application for removal of Pb(II) and Ni(II) from aqueous solution, Materials Science and Engineering: C 30 (2010) 304–310.
[23] H.T. Ngo, L.D. Tran, H.V. Tran, M.H. Do, T.D. Tran, P.X. Nguyen, Facile and solvent free routes for synthesis of size-controlable Fe_3O_4 nanoparticles, in: Proceedings of The 6th Vietnam National Conference on Solid State Physics and Materials Science (SPMS-2009), Vietnam, 8–10 November, 2009.

[24] G. Socrates, Infrared Characteristic Group Frequencies, John Wiley & Sons, New York, 1994.
[25] A. Anitha, S. Maya, N. Deepa, K.P. Chennazhi, S.V. Nair, H. Tamura, R. Jayakumar, Efficient water soluble O-carboxymethyl chitosan nanocarrier for the delivery of curcumin to cancer cells, Carbohydrate Polymers, in press, Accepted Manuscript, doi:10.1016/j.carbpol.2010.08.008.
[26] H. Yu, Q. Huang, Enhanced in vitro anti-cancer activity of curcumin encapsulated in hydrophobically modified starch, Food Chemistry 119 (2010) 669–674.
[27] M.T. Lopéz-Lopéz, J.D.G. Durán, A.V. Delgado, F. Gonzaléz–Caballero, Stability and magnetic characterization of oleate-covered magnetite ferrofluids in different nonpolar carriers, Journal of Colloid and Interface Science 291 (2005) 144–151.